Photoionization of the beryllium atom

Bin Zhou and C. D. Lin
Department of Physics, Kansas State University, Manhattan, Kansas 66506
(Received 13 June 1994)

Photoionization cross sections of the Be atom are calculated using the hyperspherical close-coupling method where a model potential is employed to approximate the screening of the $1s^2$ closed-shell core electrons. The cross sections obtained below the $Be^+(2p)$ threshold agree well with the results of other calculations and with experiment. Total and partial photoionization cross sections for photon energies between the $Be^+(2p)$ and $Be^+(3s)$ thresholds are also calculated.

PACS number(s): 32.80.Fb, 32.70.Cs, 31.50.+w, 32.80.Dz

I. INTRODUCTION

The hyperspherical close-coupling (HSCC) method has been developed recently and shown to be quite accurate and efficient in calculations of doubly excited states in two-electron atomic systems, such as He and H^-. Photoionization of such systems, in the energy range where doubly excited states interact strongly with the continuum, have been calculated and studied [1–9]. In this paper, we extend the HSCC method to calculate photoionization from atomic Be. When the photon energy is not sufficient to excite the inner $1s^2$ electrons, the Be atom can be approximated as a system of two valence electrons in the Coulomb field of the nucleus screened by the frozen closed-shell electrons. In this work, this screened Coulomb field is approximated by a simple model potential, whereby the Be atom is treated as a two-electron system in the model potential.

Photoionization of valence electrons of Be has been studied by various groups both experimentally [10] and theoretically [11–15]. But all of them are concerned with the energy range below the $Be^+(2p)$ threshold. Here we will show that for energies below the $2p$ threshold the photoionization cross sections calculated using the HSCC method agree well with other theoretical results and with experiment [10]. Moreover, we also extended the calculation to obtain photoionization cross sections between the $2p$ threshold and the $3s$ threshold. In this energy range, all partial cross sections for three open channels are presented and the cross sections are shown to be dominated by the resonances.

In the next section, a brief description of the theoretical method used for the calculation is given. The results are presented and discussed in Sec. III. A brief summary is given in Sec. IV. Atomic units are used throughout unless stated otherwise.

II. THEORETICAL METHOD AND CALCULATIONS

We write the Schrödinger equation for the two electrons in the screened Coulomb potential as

$$\left[-\frac{\nabla_1^2}{2}-\frac{\nabla_2^2}{2}-\frac{Z(r_1)}{r_1}-\frac{Z(r_2)}{r_2}+\frac{1}{r_{12}}\right]\psi(\vec{r}_1,\vec{r}_2) = E\psi(\vec{r}_1,\vec{r}_2), \quad (1)$$

where the screening of the nucleus by the inner core is approximated by an effective charge $Z(r)$ whose form is chosen to be

$$Z(r) = Z_n - Z_c + Z_c(1+a_0 r)e^{-a_0 r}, \quad (2)$$

where Z_n is the nuclear charge and Z_c is the total number of electrons in the inner core. (In the present case, $Z_n = 4, Z_c = 2$.) In the limit $r \to 0$, $Z(r) \to Z_n$ while $Z(r) \to (Z_n - Z_c)$ as $r \to \infty$. The value of the empirical parameter a_0 is determined by fitting the excited state energies of Be^+ calculated using this model potential to the experimental ones.

In hyperspherical coordinates, with the two-electron wave function expressed by $\psi(\vec{r}_1,\vec{r}_2) = \Psi(R,\alpha,\Omega)/(R^{5/2}\sin\alpha\cos\alpha)$, Eq. (1) becomes

$$\left(-\frac{1}{2}\frac{\partial^2}{\partial R^2}+\frac{H_{\rm ad}}{2R^2}-E\right)\Psi(R,\alpha,\Omega)=0, \quad (3)$$

where $R=\sqrt{r_1^2+r_2^2}$ is the hyperradius, $\alpha=\tan^{-1}\left(\frac{r_1}{r_2}\right)$ is the hyperangle, and Ω denotes collectively the four angles $(\hat{r}_1,\hat{r}_2)$. The adiabatical Hamiltonian is given by

$$H_{\rm ad}(R;\alpha,\Omega) = \Lambda^2(\alpha) + RC(\alpha,\theta_{12}), \quad (4)$$

with

$$\Lambda^2(\alpha)=\left(-\frac{\partial^2}{\partial\alpha^2}+\frac{\vec{l_1}^2}{\cos^2\alpha}+\frac{\vec{l_2}^2}{\sin^2\alpha}\right)-\frac{1}{4}, \quad (5)$$

$$C(\alpha,\theta_{12}) = -\frac{2Z(R\cos\alpha)}{\cos\alpha}-\frac{2Z(R\sin\alpha)}{\sin\alpha} + \frac{2}{\sqrt{1-\sin 2\alpha\cos\theta_{12}}}, \quad (6)$$

where θ_{12} is the angle between $\hat{r_1}$ and $\hat{r_2}$, and $\vec{l_1}$ and $\vec{l_2}$ are the individual angular momentum operators of the

two electrons.

To solve the Schrödinger equation in the HSCC method, the configuration space is divided into two regions: an inner one ($R < R_M$) where the electron-electron interaction is strong and an outer or asymptotic region ($R > R_M$) where one electron is far away from the other and the electron-electron interaction is relatively weak.

In the inner region, the hyperradius is partitioned into many small sectors $[R_0, R_1, ..., R_M]$. For a given ith sector, $R \subset [R_{i-1}, R_i]$, $\Psi(R, \alpha, \Omega)$ is expressed in a close-coupling expansion

$$\Psi(R,\alpha,\Omega) = \sum_{\mu=1}^{N_{\rm ch}} F_\mu(R)\phi_\mu(R_i^m;\alpha,\Omega) \quad (R_{i-1} < R < R_i), \tag{7}$$

where R_i^m is chosen to be at the midpoint of the sector, and $N_{\rm ch}$ channels are included. Note that channel functions ϕ_μ are *independent* of R within the sector.

Substituting (7) into the Schrödinger equation (3), one obtains the close-coupling equations for F_μ,

$$\left(-\frac{\partial^2}{\partial R^2} - 2E\right) F_\mu(R) + \sum_\nu V_{\mu\nu}(R)F_\nu(R) = 0 \qquad (\mu = 1, ..., N_{\rm ch}) \ , \tag{8}$$

where the coupling term $V_{\mu\nu}(R)$ between the channels μ and ν is given by

$$V_{\mu\nu}(R) = \frac{2}{R^2}\langle\phi_\mu(R_i^m;\alpha,\Omega)|H_{\rm ad}(R,\alpha,\Omega)|\phi_\nu(R_i^m;\alpha,\Omega)\rangle \qquad (R_{i-1} < R < R_i) \ . \tag{9}$$

The calculation in the inner region proceeds in exactly the same manner as for the pure Coulombic systems, as described in [1,2]. That is, the antisymmetrized channel functions ϕ_μ are first calculated as eigenfunctions of the adiabatic Hamiltonian $H_{\rm ad}$ and subsequently the couplings $V_{\mu\nu}(R)$ are calculated for each sector. Then starting from the innermost sector $i = 1$, the close-coupling equations (8) are integrated from R_{i-1} to R_i to obtain the radial functions $F_\mu(R)$ and the first-order derivatives with respect to R, whose values at the end point R_i are to serve as the initial boundary condition for the integration in the next sector. The integration propagates from inner sectors to outer ones, until the matching boundary $R = R_M$ is reached.

In the asymptotic region ($R > R_M$), the two-valence-electron wave function is more adequately expressed as products of wave functions of the inner valence electron bound in the screened potential and the continuum Coulomb functions for the outer valence electron in the independent electron coordinates $\vec{r_1}, \vec{r_2}$,

$$\psi_E^{(\beta)}(\vec{r_1},\vec{r_2}) = \frac{1}{r_< r_>}\sum_{i=1}^{N_{\rm ch}} \Phi_i(r_<)Y_{l_1^i l_2^i}^{LM}(\Omega) \times[f_i^E(r_>)\delta_{i\beta} - g_i^E(r_>)K_{i\beta}(E)] \qquad (\beta = 1, ..., N_{\rm ch}) \ , \tag{10}$$

where Φ_i is the radial function of the inner electron in the screened Coulomb potential for channel i characterized by the binding energy E_i of Be^+ with i represented by N and l, the inner electron's principal and angular momentum quantum number. Contrary to that of He^+ or H, the binding energies E_i of the same N for $Be^+(Nl)$ states are no longer degenerate for different angular momentum l, due to the fact that the electron is not in a pure Coulomb field. In Eq. (10), $Y_{l_1 l_2}^{LM}(\Omega)$ is the coupled spherical harmonic function formed by angular momentum l_1, l_2 of the two electrons. The functions f_i and g_i are, respectively, the energy normalized regular and irregular radial Coulomb functions of a unit charge for the outer electron if channel i is open ($E \geq E_i$), or exponentially increasing and decreasing functions if i is closed ($E < E_i$).

The reaction matrix $\vec{K}$ is obtained when the numerical solution and its derivative with respect to R in the inner region are matched with the asymptotic solutions (10) at the boundary $R = R_M$. Since the inner and outer solutions are expressed in two different coordinates, a simple frame transformation has to be made in matching.

The whole procedure outlined above has to be carried out separately for both the initial and final states to obtain the initial and final state wave functions with proper boundary conditions. Once the initial and final state wave functions are available the dipole transition matrix and thereby the photoionization cross sections of different photon energies can be calculated readily.

One problem arising from using the model potential in describing the Be atom is how to eliminate the "unphysical" occupied orbitals which are also obtained from the solution of the Schrödinger equation. In R-matrix or other diagonalization methods it is done usually by throwing away these occupied orbitals from the basis functions. In the hyperspherical approach, there are "unphysical" channels which are associated with the occupied core states. In the present case, the lowest potential curve in each symmetry is identified with a channel where the core is in the $1s$ state. In the actual Be atom, the core $1s$ orbital is occupied and thus should be excluded from the basis set for the valence electrons, but in the solution of the two-electron problem in the model potential, it is part of the complete set of basis functions. One can eliminate the core $1s$ orbital only at large R, where the amplitude of the valence-electron state associated with the core state should vanish. Thus we adopted a straightforward scheme to eliminate the effect of the undesirable occupied orbitals: In the inner region ($R < R_M$), all channels are

TABLE I. Binding energies in a.u. of discrete states of Be^+ obtained using the model potential as compared with the experimental results [16].

State	Experiment	Theory
2s	0.6691	0.66964
3s	0.2671	0.26776
4s	0.1430	0.14340
2p	0.5237	0.52430
3p	0.2294	0.22998
4p	0.1280	0.12833

included when the close-coupling equations are solved; at the matching distance $R = R_M$, the boundary condition is imposed such that the amplitudes for the lower unwanted channels vanish. Thus only the K matrices for upper (physical) channels are obtained. It should be noted that this scheme still does not rigorously exclude the effect of core states in the diabatic channels. Nevertheless the numerical results show that this scheme works well for the present calculation.

III. RESULTS AND DISCUSSIONS

In this calculation, the empirical parameter a_0 of the model potential used is 2.3436, which gives less than 0.3% error for the energies of the first few excited states of Be^+, as shown in Table I. For both the initial $^1S^e$ state and the final $^1P^o$ states, 15 channels are included. Furthermore, 150 diabatic sectors with the matching distance $R_M = 11.875$ a.u. are used in the calculation for the initial state. The binding energy obtained for the ground state Be $(2s^2)\ ^1S^e$ with respect to the Be^{2+} core is –1.012 76 a.u. (the value would be –1.036 94 a.u. if the lowest channel is completely eliminated for all R's), which is to be compared with the experimental value –1.0133 a.u. [16]. For $^1P^o$ final state wave functions, 330 diabatic sectors with $R_M = 89.5$ a.u. are used. Photoionization cross sections in both the dipole length and the dipole acceleration forms are calculated. The velocity form, which involves derivative terms, is not used since in the diabatic-by-sector method the hyperradial wave functions at the junction of the two sectors are not continuous and the numerical evaluation of the matrix elements becomes much more tedious.

In Figs. 1 and 2, the $^1S^e$ and $^1P^o$ adiabatic potential curves of Be are shown. Because the asymptotic potentials for the same N but different l are no longer degenerate, potential curves such as the $2s\epsilon s$ and $2p\epsilon p$ of the $^1S^e$ symmetry as well as the $2s\epsilon p$ and $2p\epsilon s, \epsilon d$ of the $^1P^o$ symmetry now approach different asymptotic limits, the binding energies of $Be^+(2s)$ and $Be^+(2p)$. We have calculated photoionization cross sections for two photon

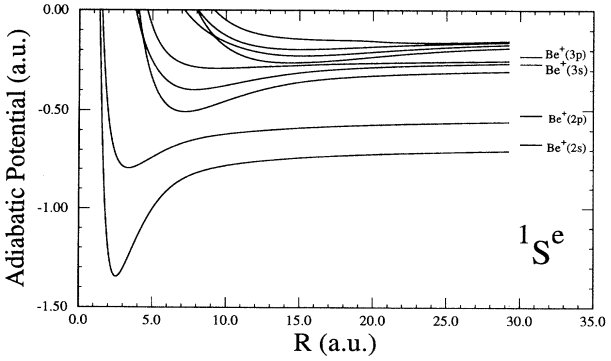

FIG. 1. Adiabatic potentials for $^1S^e$ states of Be, as functions of hyperradius R. The horizontal bars indicate the asymptotic limits of potentials.

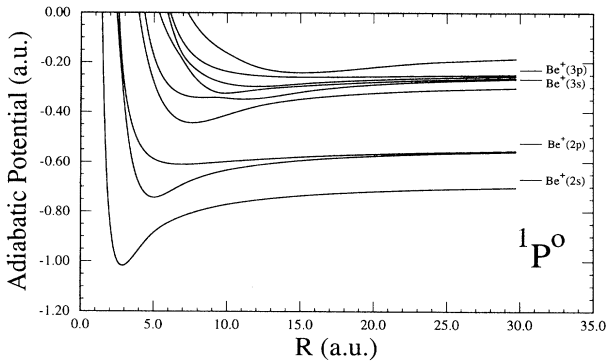

FIG. 2. Adiabatic potentials for $^1P^o$ states of Be, as functions of hyperradius R. The horizontal bars indicate the asymptotic limits of potentials.

energy ranges: (1) between the $Be^+(2p)$ and $Be^+(2s)$ thresholds; (2) between the $Be^+(3s)$ and $Be^+(2p)$ thresholds. The photoionization cross sections are displayed in terms of the total energy of the two outer electrons. Thus the corresponding photon energy is obtained by subtracting the ground state energy from the total energy.

A. Photoionization below the $Be^+(2p)$ threshold

In Fig. 3 photoionization cross sections of Be for energies below the $Be^+(2p)$ threshold (–0.5237 a.u.) but above the $Be^+(2s)$ threshold (–0.6691 a.u.) are shown, for both the length (L) and acceleration (A) gauges. The results of the two dipole gauges show reasonable agreement except for energies between –0.595 and –0.555 a.u, where the A form shows abnormally larger cross sections than the L form. This might be attributed to the limitations of the elimination scheme for the core states used here. The L-form results agree reasonably well with those of Moccia and Spizzo [14] and with the old experimental measurement [10]. The present calculation can be looked upon as an improvement of the earlier work of Greene

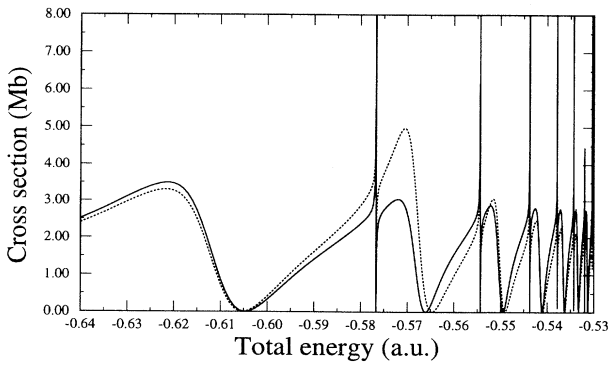

FIG. 3. The calculated photoionization cross sections of Be as functions of the total energy between the $Be^+(2s)$ and $Be^+(2p)$ thresholds. The solid line is the length form; the dotted line is the acceleration form.

[12] where he also used hyperspherical coordinates in the calculation. But his calculation coupled only a few hyperspherical adiabatic channels and the model potential he used for describing the $e^- + Be^+$ system is less accurate.

In this photon energy range (between 9.35 eV and 13.32 eV), only the $2s\epsilon p$ channel is open. Besides the direct ionization to this continuum from the ground state, there is also contribution from the autoionization of doubly excited states associated with the two $2p$ channels (see Fig. 2), which are populated when the photon energy is large enough. From the photoionization spectrum (Fig. 3), one can clearly identify two series of resonances, corresponding to the autoionization of the two Rydberg series of doubly excited states. The broad resonances represent the $2pns$ series while the narrow sharp ones represent the $2pnd$ series. The intriguing feature in this case is that autoionization widths of $2pns$ resonances are significantly larger (more than ten times) than those of the corresponding "+" series of He. This may be attributed to the fact that these resonances decay to the $2s\epsilon s$ continuum with smaller photoelectron energies. Alternatively, this is interpreted as resulting from the strong and broad *nonadiabatic* coupling between the two adiabatic channels $2p\epsilon s$ and $2s\epsilon p$ (the lowest two potential curves in Fig. 2), especially near the avoided crossing at $R = 5$. As suggested by Greene [12], this strong coupling leads to a strong mixing of the two channels with almost equal amplitudes in the two-electron wave functions.

The two lowest curves in Fig.2 may be designated as $2s\epsilon p$ and $2p\epsilon s$ channels, respectively, based on the fact that they approach 2s and 2p limits asymptotically. However, the adiabatic potential curves in the inner region have characters similar to the + and − curves in He where the + curve has an antinode in electron density near the ridge ($r_1 \approx r_2$), and the − curve has a node near the ridge [13]. Note that the strong avoided crossing is treated as a real crossing in He. Thus the curve which retains the + character is the $2s\epsilon p$ curve (the lower one) at small R, and the $2p\epsilon s$ curve at large R. In other words, the $2pns$ series is to be identified with the + series in helium, with $2s2p$ as the lowest state. The $2snp$(n$\geq$ 3) series is to be identified with the − series. For beryllium, however, the + and the − designations are not accurate, nor are the $2s\epsilon p$ and the $2p\epsilon s$ designations. The eigenstates are strong mixtures of either pair of designations. This strong admixture explains why the autoionization widths of $2pns$ resonances are much broader than the + resonances in helium where the latter decay only to the $1s\epsilon p$ continuum.

B. Photoionization between $Be^+(2p)$ and $Be^+(3s)$ thresholds

In the energy range between the $Be^+(2p)$ and $Be^+(3s)$ thresholds or photon energy range from 13.32 to 20.30 eV, numerous doubly excited states associated with the $Be^+(3s, 3p, 3d)$ thresholds can be populated. Moreover, these doubly excited states can decay to three open channels, leading to Be$(2s\epsilon p), (2p\epsilon s)$, and $(2p\epsilon d)$ continuum states.

1. Total photoionization cross section

Figure 4 shows the total photoionization cross sections in this energy range. The length-form and acceleration-form results are in reasonable agreement. From this figure, one observes many doubly excited resonance states sitting on top of a continuum background. We have also shown the energy positions (vertical bars) and total autoionization widths (horizontal bars) of the lowest few doubly excited states calculated by Bachau *et al.* [17] in the figure. It is seen that their results agree well with those from the calculated photoionization spectra here. A careful analysis of the spectra near each threshold was not carried out such that very narrow resonances may be missed in the higher energy region (total energy greater than -0.28 a.u.) in Fig. 4.

A detailed analysis of the resonance states in this energy range is more complicated than the corresponding spectra in helium. From Fig. 2, the potential curves associated with the $Be^+(n = 3)$ thresholds have numerous avoided crossings. In He, these avoided crossings can be treated diabatically such that a set of $(K,T)^A$ quantum numbers can be assigned [18] to each curve. The avoided crossings, as shown in Fig. 2, are not purely diabatic for Be. However, the first two resonances in Fig. 4 appear to be associated with the curve which approaches the $3s$ threshold of Be^+ at large R. This curve, if taken adiabatically, has the + character at small R. These + states decay readily and exhibit large autoionization widths. The third resonance, which is at about -0.30 a.u., is very narrow, and is likely to be associated with the − curve at small R. In other words, it is associated with the third lowest curve at small R (see Fig. 2) among the five curves that converge to the n=3 limit of Be^+. We must emphasize, however, because of the avoided crossings, each state cannot be assigned solely to be associated with any particular adiabatic or diabatic curve. A systematic study of the spectra and the nature of each resonance in this region can be obtained only after a careful analysis of the wave functions and the corresponding parameters in the

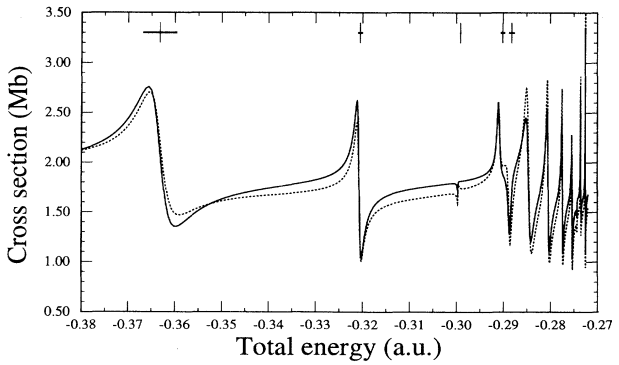

FIG. 4. The calculated total photoionization cross sections of Be as functions of the total energy between the $Be^+(2p)$ and $Be^+(3s)$ thresholds. The solid line is from the length form; the dotted line is from the acceleration form. The vertical (horizontal) bars indicate the energy positions (total autoionization width) of doubly excited states calculated by Bachau *et al.* [17].

multichannel quantum defect theory [15]. Since no experimental data are in existence at present for this energy region, such an analysis is not carried out here.

2. Partial cross sections

The breakdown of the total cross sections into three partial cross sections $\sigma_{2s\epsilon p}, \sigma_{2p\epsilon s}$, and $\sigma_{2p\epsilon d}$ is shown in Fig. 5. It is clear that the background cross section of $\sigma_{2s\epsilon p}$ is significantly larger than the other two. This is expected from the independent electron picture, because the direct ionization from the ground state $(2s^2)$ to $(2s\epsilon p)$ can be thought of as a dipole-allowed single-electron transition, while photoionization to the other two continuum channels involves two-electron transitions. We also note that the resonance profiles for each resonance, particularly the higher ones, change drastically among the three different channels.

IV. CONCLUSIONS

Using the model potential approach in the HSCC method, we have calculated photoionization cross sections from the ground state of Be. Our results agree reasonably well with existing theoretical and experimental results for energies between the $Be^+(2p)$ and $Be^+(2s)$ thresholds. Results for higher energies, between the $Be^+(3s)$ and $Be^+(2p)$ thresholds, are also presented. Due to the strong couplings among adiabatic channels, the adiabatic approximation (or diabatic representation) no longer provides a good representation of the doubly excited states for Be. The quantum numbers K, T, and A used for describing doubly excited states in helium still show relevance in discussing doubly excited states in Be, but they cannot be treated as almost "pure" quantum numbers as in He. From the hyperspherical viewpoint, the K, T, and A quantum numbers are still useful for describing properties of doubly excited states in the small-R region, which are then reflected in properties such as autoionization widths [19] and photoabsorption cross sections. On the other hand, the energy levels are determined to a large extent, especially the Rydberg states, by the potential curves at large R, such that the designation of states for Rydberg levels in terms of independent particle notation is appropriate. For a complete description of the spectra of Be, calculations should be carried out which account for both regions of the configuration space adequately. The HSCC method provides such a means for carrying out such calculations.

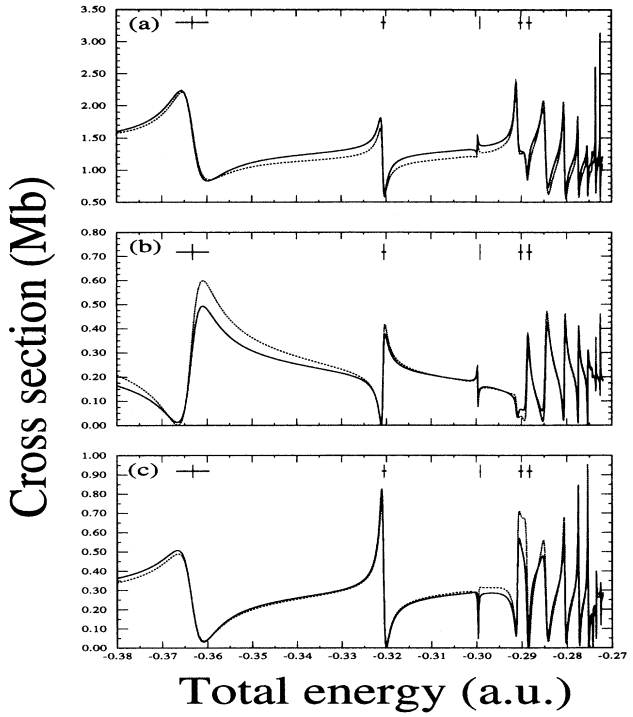

FIG. 5. The calculated partial cross sections of photoionization from Be for energy between the $Be^+(2p)$ and $Be^+(3s)$ thresholds: (a) $\sigma_{2s\epsilon p}$; (b) $\sigma_{2p\epsilon s}$; (c) $\sigma_{2p\epsilon d}$.

ACKNOWLEDGMENTS

This work was supported in part by the U.S. Department of Energy, Office of Energy Research, Office of Basic Energy Sciences, Division of Chemical Sciences. We thank J.Z. Tang, S. Watanabe, and M. Matsuzawa for helpful discussions and comments.

[1] J.Z. Tang, S. Watanabe, M. Matsuzawa, and C.D. Lin, Phys. Rev. Lett. **69**, 1633 (1992).
[2] B. Zhou and C.D. Lin, J.Z. Tang, S. Watanabe, and M. Matsuzawa, J. Phys. B **26**, 2555 (1993).
[3] B. Zhou and C.D. Lin, J. Phys. B **26**, 2575 (1993).
[4] J.-Z. Tang, S. Watanabe, and M. Matsuzawa, Phys. Rev. A **46**, 2437 (1992).
[5] J.-Z. Tang, S. Watanabe, M. Matsuzawa, and C. D. Lin, Phys. Rev. Lett. **69**, 1633 (1992).
[6] B. Zhou, C.D. Lin, J.-Z. Tang, S. Watanabe, and M. Matsuzawa, J. Phys. B **26**, L337 (1993).
[7] B. Zhou and C.D. Lin, Phys. Rev. A **49**, 1057 (1994).
[8] J.-Z. Tang, Y. Wakabayashi, M. Matsuzawa, S. Watanabe, and I. Shimamura, Phys. Rev. A **49**, 1021 (1994).
[9] J.-Z. Tang and I. Shimamura, Phys. Rev. A **50**, 1321 (1994).
[10] G. Mehlman-Balloffet and J.M. Esteva, Astrophys. J. **157**, 945 (1969).
[11] J. Dubau and J. Wells, J. Phys. B **6**, L33 (1973).
[12] C.H. Greene, Phys. Rev. A **23**, 661 (1981).
[13] C.D. Lin, J. Phys. B **16**, 723 (1983).
[14] R. Moccia and P. Spizzo, J. Phys. B **18**, 3537 (1985).
[15] U. Fano and A.R.P. Rau, *Atomic Collisions and Spectra* (Academic Press, New York, 1986).
[16] R.L. Kelly, Oak Ridge National Laboratory Report No. ORNL-5922, 1982 (unpublished).
[17] H. Bachau, P. Galan, F. Martin, A. Riera, and M. Yanez, At. Data Nucl. Data Tables **44**, 305 (1990).
[18] C.D. Lin, Phys. Rev. A **29**, 1019 (1984).
[19] Z. Chen and C.D. Lin, J. Phys. B **22**, 2875 (1989).